Proceedings of CONF-MPCS 2026 Symposium: Theoretic Physics and Plasma Physics
DOI: 10.54254/2753-8818/2026.DL32089

Spectral Reflectivity Uniformity of Metal Meshes for Far Infrared Fabry–Perot Interferometers

Litong Xu

York university, Toronto, Canada
m18701382690@hotmail.com

Abstract. Metal meshes are commonly used as reflective elements in far infrared astronomical instruments, where spectrally uniform reflectivity is important for stable Fabry–Perot interferometer performance and reliable calibration. In this work, we quantitatively compare the spectral reflectivity uniformity of representative metal mesh geometries using full wave electromagnetic simulations. Square and circular meshes with inductive and capacitive topologies are analyzed over the 200 to 400 GHz band. A figure of merit based on the normalized root mean square deviation of reflectance from a target value is used to evaluate spectral flatness. Parameter sweeps over lattice pitch and normalized feature size reveal well defined regions that minimize spectral variation. All four geometries can achieve comparable reflectivity uniformity when properly optimized, with square inductive meshes yielding the lowest figure of merit within the explored design space. The results provide practical guidance for selecting metal mesh geometries with flat reflectance profiles in far infrared Fabry–Perot interferometers and related optical systems.

Keywords: Metal Mesh, Fabry-Perot Interferometer, Spectral Reflectivity, Frequency Selective Surface

1. Introduction

Metal meshes are periodic conductive structures that exhibit frequency-dependent reflection and transmission characteristics determined by their geometry, periodicity, and material composition [1]. Typically fabricated through lithographic patterning or photochemical etching of thin metallic films, these meshes act as frequency-selective surfaces (FSS) that can function as reflective mirrors, band-defining filters, or polarizing elements across microwave to far-infrared and terahertz wavelengths. Their ability to control electromagnetic response by geometric design rather than by material dispersion makes them particularly attractive for cryogenic and spaceborne optical systems, where conventional multilayer coatings often suffer from thermal mismatch or poor adhesion.

In astronomical instrumentation, metal meshes are commonly used as reflective components in Fabry-Perot interferometers (FPIs) and broadband filters [2]. Examples include their application in CCAT-prime [3], Herschel SPIRE [4], HIWIND [5], SPIFI [6], FIFI [7] and KWIC [8]. For these applications, maintaining flat reflectance across the operational frequency range is essential. Uniform reflectivity ensures stable finesse and throughput in FPIs and prevents spurious features in

DOI: 10.54254/2753-8818/2026.DL32089

reflective filters. Significant variation in reflectance with wavelength can degrade spectral resolution, disrupt the regularity of transmission peaks, and complicate subsequent data processing.

Achieving spectrally flat response is challenging. The reflectivity of metal meshes is influenced by multiple geometric factors and electromagnetic effects, including diffraction, resonance, and substrate interactions. Traditional design approaches often rely on simplified analytical models or empirical guidelines. While these methods suffice for estimating characteristic frequencies, they are inadequate for predicting fine spectral structure over wide bandwidths.

This study presents a systematic and quantitative evaluation of spectral reflectivity uniformity for several mesh patterns. By systematically varying geometric parameters, we identify trends in absolute reflectance and spectral flatness across these patterns. The results provide practical guidance for designing mesh reflectors in next-generation astronomical instruments.

2. Methods

We use full-wave electromagnetic simulations in CST Studio Suite to compute the spectral reflectivity of metal mesh patterns. Each design is represented by a single periodic unit cell with lateral unit-cell (periodic) boundaries and Floquet ports on the input and output faces to model an infinitely extended surface under plane-wave illumination [9]. The simulation outputs complex scattering parameters, where S_{11} denotes the reflection coefficient at the input port (ratio of the reflected to incident electric field amplitudes) and S_{21} denotes the transmission coefficient at the output port (ratio of the transmitted to incident amplitudes). From these parameters, the power reflectance is calculated as $R = |S_{11}|^2$, using power-wave normalization at the Floquet ports. Energy conservation is verified by confirming $R + T + A \approx 1$, where $T = |S_{21}|^2$ represents transmittance and A accounts for ohmic and dielectric losses as reported by the solver.

Without loss of generality, we focus on the 200–400 GHz band. This sub-band approximates the 210–420 GHz coverage of the CCAT EoR-Spec FPI and is representative of far-infrared and submillimeter instruments that use mesh mirrors or reflective filters [10]. In such FPIs the mirror reflectivity often varies with frequency, which can complicate calibration and data reduction. Studying spectral flatness in 200–400 GHz therefore serves both as a realistic and broadly useful test window.

For each geometry, CST models are scripted from a common template so that ports, boundaries, material models, mesh settings, and solver tolerances are identical across runs. Metals are assigned finite conductivity; dielectric substrates, when present, are assigned refractive index and small loss tangent.

To quantify spectral uniformity we define a figure of merit (FOM) that penalizes deviations of the reflectance from a target value R_0:

$$\mathrm{FOM} = \sqrt{\frac{1}{f_2 - f_1}\int_{f_1}^{f_2}\left[\frac{R(f)-R_0}{R_0}\right]^2 \mathrm{d}f}. \tag{1}$$

In this study the frequency interval is $[f_1, f_2] = [200,400]$ GHz and the target reflectivity is set to $R_0 = 0.90$. We choose $R_0 = 0.90$ because high-reflectance mirrors are typical in astronomical FPIs and because such a value yields a reasonably high cavity finesse. For a simple lossless two-mirror FPI, the ideal finesse scales as $\mathscr{F} \approx \frac{\pi\sqrt{R}}{1-R}$ [11]. We use full-wave electromagnetic simulations in CST Studio Suite to compute the spectral reflectivity of metal mesh patterns. Each design is represented by a single periodic unit cell with lateral unit-cell (periodic) boundaries and Floquet

DOI: 10.54254/2753-8818/2026.DL32089

ports on the input and output faces to model an infinitely extended surface under plane-wave illumination. The simulation outputs complex scattering parameters, where S_{11} denotes the reflection coefficient at the input port (ratio of the reflected to incident electric field amplitudes) and S_{21} denotes the transmission coefficient at the output port (ratio of the transmitted to incident amplitudes). From these parameters, the power reflectance is calculated as We use full-wave electromagnetic simulations in CST Studio Suite to compute the spectral reflectivity of metal mesh patterns. Each design is represented by a single periodic unit cell with lateral unit-cell (periodic) boundaries and Floquet ports on the input and output faces to model an infinitely extended surface under plane-wave illumination [9]. The simulation outputs complex scattering parameters, where S_{11} denotes the reflection coefficient at the input port (ratio of the reflected to incident electric field amplitudes) and S_{21} denotes the transmission coefficient at the output port (ratio of the transmitted to incident amplitudes). From these parameters, the power reflectance is calculated as so keeping R near 0.9 maintains $\mathscr{F}$ in a range that supports the resolving powers commonly used in far-infrared spectroscopy [8]. With Eq. (1), a lower FOM means the spectrum $R(f)$ stays closer to the desired flat level R_0 across the band; a higher FOM indicates stronger spectral structure.

The workflow is: (i) programmatically build the unit-cell geometry in CST from a small set of inputs; (ii) assign materials and boundary conditions; (iii) solve for S -parameters over 200–400 GHz with adaptive meshing and de-embedding to the mesh plane; (iv) compute $R(f)$ and verify energy closure and port-mode cutoff conditions; and (v) post-process $R(f)$ to evaluate Eq. (1). This pipeline allows efficient sweeps over geometry inputs (to be detailed in the next section) while preserving consistent solver settings and reproducibility.

3. Simulation structures and results

The simulation structures considered in this study are shown in Fig. 1. Due to practical limitations on computational time, we restrict our analysis to four representative metal mesh geometries: square inductive, square capacitive, circular inductive, and circular capacitive meshes. Although more complex or hybrid patterns can be conceived, these four cases span the two fundamental electromagnetic response types of frequency-selective surfaces—inductive and capacitive—and therefore provide a meaningful basis for comparative analysis of spectral reflectivity uniformity.

DOI: 10.54254/2753-8818/2026.DL32089

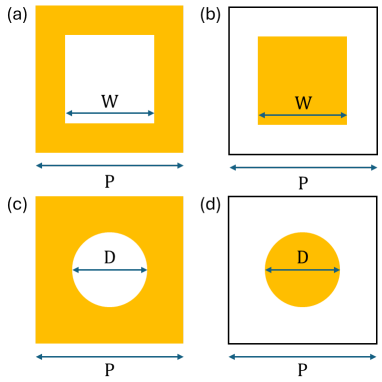

Figure 1. Unit-cell geometries of metal mesh patterns used in the CST simulations: (a) square inductive mesh, (b) square capacitive mesh, (c) circular inductive mesh, and (d) circular capacitive mesh. The yellow regions represent the metallic structures, while the white regions denote vacuum. For each unit cell, P denotes the lattice pitch, and W or D denotes the characteristic feature size of the mesh. In the simulations, only two geometric parameters were varied: the pitch P and the normalized feature-size ratio, defined as W/P or D/P

For each geometry, full-wave electromagnetic simulations were performed by sweeping the lattice pitch P and the normalized feature-size ratio (W/P or D/P). The resulting reflectance spectra were evaluated using the FOM defined in Eq. (1), which quantifies the normalized root-mean-square deviation of the reflectance from the target value $\mathrm{R}_0 = 0.9$ over the 200–400 GHz band. The resulting FOM values are summarized as contour maps in Fig. 2.

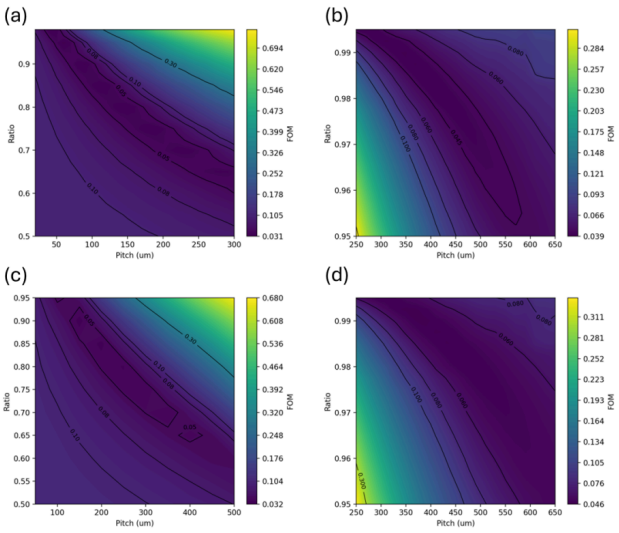

Figure 2. Contour plots of the reflectivity uniformity FOM. The FOM depends on lattice pitch P and normalized feature-size ratio. There are four metal mesh configurations in the figure: (a) square inductive mesh, (b) square capacitive mesh, (c) circular inductive mesh, and (d) circular capacitive mesh. For square meshes, the ratio is W/P. For circular meshes, the ratio is D/P. A lower FOM value means a flatter reflectance spectrum between 200 GHz and 400 GHz. Pronounced valleys appear in the contour plots. These valleys mean there are optimal points in the two-dimensional parameter space. These points can maximize spectral reflectivity uniformity

DOI: 10.54254/2753-8818/2026.DL32089

All four configurations have contour plots with pronounced valley-like features. These features are in the two-dimensional parameter space. This shows that the parameter scans work well. They find the local minima of the FOM. These minima correspond to mesh configurations. These configurations can maximize spectral reflectivity uniformity. The valleys also show that a flat reflectance spectrum is not easy to get. It is not enough to just scale the pitch or feature size of the mesh. We need to balance geometric and electromagnetic effects carefully.

We compared the four geometries. Their minimum FOM values are similar. This means all four geometries can achieve similar spectral uniformity when optimized. Among the four, the square inductive mesh has the lowest FOM value in the explored parameter range. This shows metallic grids with connections have more stable broadband reflectance. They are better than isolated patch-type geometries under current design constraints. One possible reason is that inductive meshes can keep current flowing along the metal surface. This reduces spectral oscillations in reflectivity. These oscillations are caused by frequency-dependent resonances. Capacitive meshes are different. They accumulate charge between metal patches. This may lead to stronger frequency dispersion around geometric resonances.

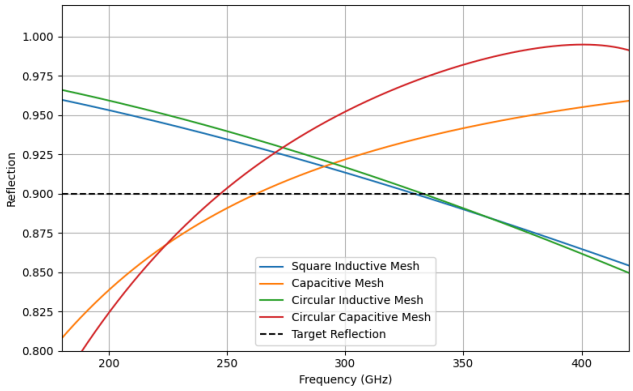

Figure 3. Simulated reflectance spectra for the minimum-FOM designs of the four metal mesh geometries. The dashed black line marks the target reflectivity$R_0 = 0.9$used in the FOM definition. Inductive and capacitive meshes have distinctly different spectral behaviors over the band, while all optimized geometries achieve a similar degree of reflectivity uniformity around the target value

Fig. 3 plots the reflectance spectra for the minimum-FOM designs of the four geometries. It is seen that all optimized geometries maintain reflectance around the target value of $R_0 = 0.9$ for a large part of the band, independent of their topologies. There are also distinct differences between inductive and capacitive meshes. The inductive meshes have a monotonic decrease in reflectance with increasing frequency, while the capacitive meshes have an increasing reflectance towards higher frequencies. These are consistent with the expected inductive and capacitive behaviors of the connected grids and isolated patches, respectively.

The similarity in the achievable values of FOM for different geometries indicates that, for such simple periodic structures, the spectral reflectivity uniformity is dominated by global parameters like effective fill factor and electrical periodicity, rather than the details of the unit cell geometry. This also indicates that, for the class of simple inductive and capacitive meshes, the geometric topology is of secondary importance compared to the normalized scaling parameters. Such differences may become more pronounced for more complex designs, which are not considered in this study.

In summary, these results show that the method of systematic exploration of parameter space, together with a quantitative measure of uniformity, is an effective tool for choosing metal mesh

DOI: 10.54254/2753-8818/2026.DL32089

layouts with flat spectral reflectivity. This technique is directly applicable to the design of Fabry-Perot interferometer mirrors and reflective filters for far-infrared astronomy.

4. Conclusion and outlook

This work presents a systematic simulation-based comparison of spectral reflectivity uniformity for typical metal mesh geometries used in astronomical applications. Using full-wave electromagnetic simulations and a clearly defined FOM, four representative layouts were evaluated over a frequency range relevant to far-infrared Fabry-Perot interferometers.

By varying lattice pitch and feature size ratio, distinct regions with reduced spectral variation were identified within the parameter space. After optimization, all four geometries achieved comparable performance, with the square inductive mesh exhibiting the lowest FOM within the explored range.

The results indicate that spectral reflectivity uniformity can be efficiently optimized through systematic parameter sweeps. A small set of geometric parameters is sufficient to characterize basic mesh layouts. The proposed FOM serves as a practical quantitative tool for comparing structures and guiding early-stage design of reflective elements in Fabry-Perot interferometers and related systems.

Several extensions could strengthen this framework. First, the structural space could be expanded to include more complex lattice symmetries or hybrid connected-isolated designs, which might yield lower FOM values or enhanced robustness. Second, incorporating angle-dependent response into the FOM definition would better represent real optical systems where incident radiation spans a finite angular range. Finally, experimental validation through free-space reflectance measurements is necessary to quantify deviations between simulation and fabricated samples and to refine modeling assumptions.

In summary, this study establishes a clear quantitative basis for evaluating and optimizing spectral reflectivity uniformity in metal meshes. The methodology can be extended to more realistic operating conditions and broader structural spaces, supporting the development of high-performance reflective components for far-infrared and submillimeter astronomical instrumentation.

References

[1] R. Ulrich, "Far-infrared properties of metallic mesh and its complementary structure, " Infrared Physics, vol. 7, no. 1, pp. 37–55, 1967.

[2] P. A. Ade, G. Pisano, C. Tucker, and S. Weaver, "A review of metal mesh filters, " Millimeter and Submillimeter Detectors and Instrumentation for Astronomy III, vol. 6275, pp. 248–262, 2006.

[3] T. Nikola, S. K. Choi, C. J. Duell, et al., "Ccat-prime: The epoch reionization spectrometer for primce-cam on fyst, " in Millimeter, Submillimeter, and Far-Infrared Detectors and Instrumentation for Astronomy XI, SPIE, vol. 12190, 2022, pp. 247–262.

[4] M. J. Griffin, A. Abergel, A. Abreu, et al., "The herschel-spire instrument and its in-flight performance, " Astronomy & Astrophysics, vol. 518, p. L3, 2010.

[5] Wu, Q., Wang, W., Roble, R.G., Häggström, I. and Strømme, A. "First daytime thermospheric wind observation from a balloon-borne Fabry-Perot interferometer over Kiruna (68N)". Geophysical Research Letters, 39(14), 2012.

[6] Bradford, C.M., Stacey, G.J., Swain, M.R., Nikola, T., Bolatto, A.D., Jackson, J.M., Savage, M.L., Davidson, J.A. and Ade, P.A. "SPIFI: a direct-detection imaging spectrometer for submillimeter wavelengths". Applied Optics, 41(13), pp.2561-2574, 2002.

[7] Poglitsch, A., Beeman, J.W., Geis, N., Genzel, R., Haggerty, M., Haller, E.E., Jackson, J., Rumitz, M., Stacey, G.J. and Townes, C.H. The MPE/UCB far-infrared imaging Fabry-Perot interferometer (FIFI). International journal of infrared and millimeter waves, 12(8), pp.859-884, 1991.

DOI: 10.54254/2753-8818/2026.DL32089

[8] Stacey, G.J., Gull, G.E., Hayward, T.L., Latvakoski, H. and Peng, L. KWIC imaging of the Orion Nebula. In From Gas to Stars to Dust (Vol. 73) , 1995.
[9] B. A. Munk, Frequency selective surfaces: theory and design. John Wiley & Sons, 2005.
[10] N. F. Cothard, S. K. Choi, C. J. Duell, et al., "The design of the ccat-prime epoch of reionization spectrometer instrument, " Journal of low temperature physics, vol. 199, no. 3, pp. 898–907, 2020.
[11] M. Born and E. Wolf, Principles of optics: electromagnetic theory of propagation, interference and diffraction of light. Elsevier, 2013.